Renewable and Sustainable Energy Reviews 31 (2014) 353–367

Contents lists available at ScienceDirect

Renewable and Sustainable Energy Reviews

journal homepage: www.elsevier.com/locate/rser

Dehydroxylation of serpentine minerals: Implications for mineral carbonation

Bogdan Z. Dlugogorski [a,c,*], Reydick D. Balucan [a,b]

[a] Priority Research Centre for Energy, The University of Newcastle, Callaghan, NSW 2308, Australia
[b] School of Chemical Engineering, The University of Queensland, QLD 4072, Australia
[c] School of Engineering and Information Technology, Murdoch University, WA 6150, Australia

ARTICLE INFO

Article history:
Received 14 August 2012
Accepted 11 November 2013
Available online 31 December 2013

Keywords:
CO_2
Mineralisation
Antigorite
Chrysotile
Lizardite
Serpentine
Dehydroxylation

ABSTRACT

This review examines studies on the dehydroxylation of serpentine minerals published in the open literature from 1945 to 2013, with brief description of earlier work. Presently, the energy cost and technological complications, required to amorphise serpentine minerals by dehydroxylation, prevent their large-scale application for sequestering of CO_2. The focus of the review is on thermal dehydroxylation, although mechanical dehydroxylation by grinding and shock, as well as thermomechanical dehydroxylation are also covered. We discuss the chemical and physical transformations involving the proposed mechanisms, thermal stability, reaction kinetics, the formation of intermediates and products, associated heat requirements, factors that influence the reaction, as well as associated enhancements in both dissolution and carbonation. The primary factor controlling the availability of Mg for either extraction or carbonation is structural disorder. The review demonstrates that, activation processes must avoid recrystallisation of disordered phases to fosterite and enstatite, and minimise the partial pressure of water vapour that engenders reverse reaction.

Contents

Abbreviations: AEM, analytical electron microscopy; ARC, Albany Research Center; C_p^{aver}, average heat capacity; DSC, differential scanning calorimetry; DTG, derivative thermogravimetry; DTA, differential thermal analysis; E_a, apparent activation energy; EGA, evolved gas analysis; FTIR, Fourier transform infrared spectroscopy; KCE, kinetic compensation effect; MAS NMR, magic angle spinning nuclear magnetic resonance; P_{H2O}, partial pressure of water; SEM, scanning electron microscopy; TGA, thermogravimetric analysis; TG, thermogravimetric; Q_{latent}, latent heat requirement; $Q_{sensible}$, sensible heat requirement; Q_{total}, total heat requirement; XRF, X-ray fluorescence; XRPD, X-ray powder diffraction; % OH_{res}, percent residual hydroxyl content

* Corresponding author. Tel.: +61 8 9360 6770.
E-mail address: B.Dlugogorski@murdoch.edu.au (B.Z. Dlugogorski).

1364-0321/$ - see front matter © 2013 Elsevier Ltd. All rights reserved.
http://dx.doi.org/10.1016/j.rser.2013.11.002

1. Introduction

Studies on serpentine minerals span more than century-old experimental investigations and very recent quantum physics modelling. Thermal studies performed as early as 1920s, and reported in Refs. [1,2], identified the decomposition products and changes in phase composition [1,2], mainly for geological and limited number of industrial applications [3–11]. A much early set of work, focused on the chemical composition, structure and varieties of natural samples, predates these thermal studies [12,13], with investigations dating back to as early as 1834. The studies on the thermal behaviour of serpentines involved applications of thermoanalytical methods such as thermogravimetry (TGA), derivative thermogravimetry (DTG), differential thermal analysis (DTA), differential scanning calorimetry (DSC) and evolved gas analysis (EGA). These methods were often applied in conjunction with physicochemical or compositional analysis, X-ray powder diffraction (XRPD), X-ray fluorescence (XRF), scanning electron microscopy (SEM), analytical electron microscopy (AEM), Fourier transform infrared, as well as Raman and magic angle spinning nuclear magnetic resonance spectroscopy (FTIR, Raman, MAS NMR).

With the discontinued use of chrysotile asbestos for thermal insulation, the industrial consumption of these minerals has been limited to fillers in steel making and as alternate sources of Mg. The emergence of mineralisation of CO_2 as a permanent solution for storing its anthropogenic emissions presents a renewed industrial interest in utilisation of this abundant resource [14–20]. It has been demonstrated that, the direct aqueous carbonation of thermally treated serpentines is a technically feasible option for CO_2 storage, albeit the process remains proven only at a laboratory scale, [21,22] with engineering scale-up design calculations projecting the present cost as at least \$70 t^{-1} CO_2 (net) [23]. Although thermal activation improves the extent of serpentines' conversion to carbonates, this process requires substantial energy input and may not guarantee high degree of carbonation [16,17,21,22,24–26].

After the preliminary section describing the serpentine minerals, this review provides the necessary background on the dehydroxylation of serpentine minerals and discusses associated concepts of particular significance to mineral carbonation. It evaluates published studies of these minerals to identify the treatment conditions and types of dehydroxylated mineral phases formed that increase the reactivity of treated serpentines for their reaction with CO_2. Heating, grinding and shocking of serpentine minerals dehydroxylate them, resulting in the amorphisation of their structure. Sonication facilitates more efficient dehydroxylation, but cannot induce dehydroxylation on its own. When applied concurrently with heating, grinding significantly improves the activation process and reduces its severity. This approach is denoted as the thermomechanical activation. The thermal activation is reviewed first, followed by the analyses of other dehydroxylation techniques. This leads to review of practical considerations of energy requirements, carbonation efficiency, and technological processes that have been proposed to dehydroxylate serpentine minerals, to make them useful for sequestering CO_2.

2. Serpentine minerals

Serpentine minerals are 1:1 layered hydrated magnesium silicates, with a typical MgO and SiO_2 content of 35–40% each and water content of ~12% [27–30]. They are Mg analogues of kaolinite, consisting of alternating tetrahedral (silica-like) and octahedral (brucite-like) sheets (Fig. 1). The distinct structural variations lead to three principal polymorphs; namely, antigorite, chrysotile and lizardite [28–34]. Although, these three minerals have similar chemical compositions [13,30], they differ in structural stacking arrangements [30,33,34]. Serpentine minerals contain 12.1–13.5$\%_{w/w}$ H_2O, 41.0–42.1$\%_{w/w}$ SiO_2, 38.3–40.9$\%_{w/w}$ MgO, with Fe_2O_3/FeO ratios ranging from 0.31 to 9.78. Based on the compiled analyses of serpentines published between 1834 and 1962 [12], chemical differences exist amongst these minerals [13]. Antigorite has relatively low H_2O but high SiO_2 content, chrysotile high H_2O and MgO abundances (40.93$\%_{w/w}$) but with small ratio of Fe_2O_3 to FeO, whilst lizardite exhibits high SiO_2 but low FeO content [13]. Lizardite and chrysotile follow an idealised formula of ($Mg_3Si_2O_5(OH)_4$) [27,28,30], but the former possesses a planar

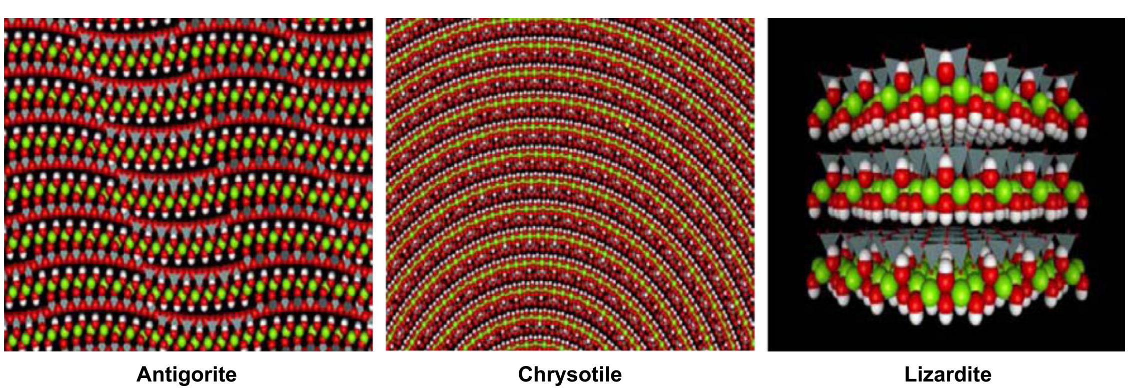


Fig. 1. The structures of antigorite, chrysotile and lizardite [30,41]. The Mg, O and H atoms of the octahedral layer are represented by green, red and white spheres, respectively. The grey tetrahedra represent the silica layer. Note the wave-like pattern of antigorite, parallel sheets for lizardite and concentric structure of chrysotile. (For interpretation of the references to colour in this figure caption, the reader is referred to the web version of this article.)

structure [27,30,35,36] whilst the latter displays a concentrically layered arrangement [27,30]. Antigorite, on the other hand, deviates from the idealised composition towards a chemical formula of ($Mg_{48}Si_{34}O_{85}(OH)_{62}$), [27,28,37] that affords a modulated structure to accommodate structural misfits [27,30,37–40].

Serpentines form in the exothermic hydration of peridotites, in a process called serpentinisation [27–30,42]. Peridotites are heavy ultramafic rocks that are found mainly in the Earth's mantle and include olivine and pyroxene minerals. The resulting serpentine minerals have lower density (2.6 g cm^{-3}) than their parent minerals (e.g., density of olivine is 3.3 g cm^{-3}) due to the volume increase during hydration. Serpentines represent rock forming minerals [30] wherein the rocks composed mainly of serpentine minerals are called serpentinites. Accessory minerals commonly found in these rocks comprise magnetite, brucite, carbonates and relict peridotitic minerals forsterite (Mg_2SiO_4) as well as enstatite ($MgSiO_3$).

Serpentine minerals and peridotitic minerals constitute candidate feedstocks for the industrial mineralisation of CO_2 [16,17,19]. Comparing these minerals, the magnesium dissolution coefficients, at 25 °C and in a wide pH range, decrease according to the following order: forsterite > serpentine > enstatite [43]. This trend in magnesium availability reflects the observed enhancement in the conversion of these ultramafic minerals to carbonates [44]. The Mg dissolution coefficients can be viewed as an indication pertaining to the relative short-time dissolution rates of the three minerals. This trend is based on the measured dissolution rates by Luce et al. [43]. No study, using similar conditions as those of Luce [43] has measured the dissolution rates of thermally activated serpentine. As such, it is not yet possible to include activated serpentine in the ranking based on the generalised Mg dissolution trend amongst these minerals.

3. Thermal activation

3.1. Thermal stability

Thermal decomposition of serpentine is a dehydroxylation reaction where structurally bound hydroxyls are removed from the solid and liberated as water vapour. This reaction generally occurs above 500 °C. Each serpentine polymorph, however, differs in the thermal stability and thus possesses a different decomposition temperature. The characteristic decomposition temperatures for lizardite, chrysotile and antigorite, as determined from the DTG peak, were first reported to correspond to 635, 664 and 700 °C, respectively [45]. However, recent DTG and DTA studies showed higher thermal stability of lizardite than chrysotile, with peak temperatures of 715 and 720 °C for antigorite, 708 and 714 °C for lizardite, 685 and 691 °C for polygonal serpentine, as well as 650 and 654 °C for chrysotile [46]. Whilst, in the results of most investigations, one readily distinguishes antigorite as a consequence of its high decomposition temperature (> 700 °C) coupled to a diagnostic signal at 740–760 °C, the decomposition temperatures for chrysotile and lizardite overlap each other (600–700 °C). Polygonal serpentine, which is an intermediate structure between lizardite and chrysotile and consists of polygonally stacked flat layers of both minerals [27], has a higher thermal stability than chrysotile but lower than lizardite [46].

Heat transport properties of serpentine minerals highly depend on their water content. The thermal diffusivity and conductivity decrease with increasing temperature. Fig. 2 illustrates that, the thermal conductivity of serpentinite tends to oscillate with temperature, displaying peaks at around 177 and 577 °C. These peaks indicate the release of water in the dehydration and dehydroxylation reactions, respectively [47]. Whilst the thermal stability of serpentine minerals primarily emanates from the structurally bound water, physisorbed and chemisorbed waters also influence stability. The latter is directly linked to the particle size and partial pressure of water [3,48,49]. Pressure of water vapour, P_{H2O}, as low as 0.1 Pa and extremely small particles decrease the rate of liberation of water from these minerals. Small particles, which are highly dense and compacted, need to be fluidised, to avoid entrapment of liberated water. Similarly, water vapour present in the inter-particle spaces may inhibit the liberation of water from minerals, by promoting the reverse reactions that increase in importance with increasing local concentration of water vapour.

Thermal stability also depends on the type of thermal treatment that normally entails either isothermal or prograde heating; the latter involving ramping up the temperature, usually at a constant rate. Thermal events are typically observed at higher temperatures in prograde heating experiments, whilst these events occur at a much lower temperature in isothermal studies. Table 1 summarises the thermal events occurring in heated

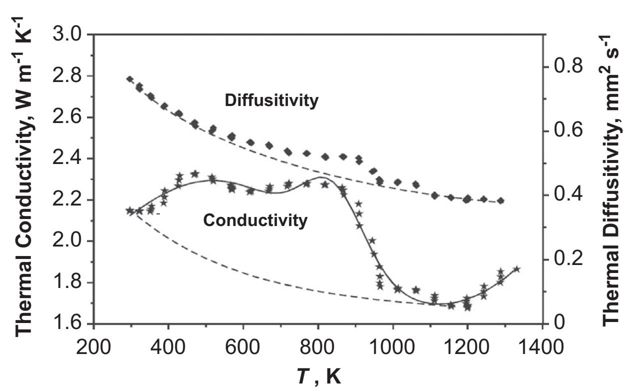


Fig. 2. Temperature dependence of thermal conductivity and diffusivity of a serpentinite sample [47].

Table 1
Summary of the differences in treatment temperature and duration for prograde and isothermal heating.

Type of heating	Mineral	Thermal event	*T* (°C)	*t* (h)	Ref.
Prograde	70% Lizardite	Dehydration of adsorbed water	100–140	« 1	[50]
	15% Chrysotile	Brucite dehydroxylation	400–420	« 1	
	6% Brucite	Serpentine dehydroxylation	620–690	« 1	
		Ordering of metaserpentine phase	790–820	« 1	
		Forsterite formation	790–820	« 1	
Isothermal	Chrysotile	Forsterite formation	500	30824	[3]
		Forsterite formation	550	16	
		Full dehydroxylation	600	4	
	Antigorite	Full dehydroxylation	660	3	51
	Lizardite	Full dehydroxylation	650	2	[52]
	Lizardite, Antigorite, Chrysotile	Full dehydroxylation	575–600	12	[53]
		Forsterite formation	575–600	12	

serpentines depending on the type of thermal treatment. For example, a serpentinite sample (70% lizardite, 15% chrysotile, 6% brucite, 5% magnetite and 4% carbonates, particle diameter <0.1 mm, sample weight 0.1 g, heating rate 10–20 °C min^{-1}) subjected to prograde heating in air exhibits dehydration of adsorbed water between 100 and 140 °C, brucite dehydroxylation from 400 to 420 °C, serpentine dehydroxylation from 620 to 690 °C, ordering of meta-serpentine structure and formation of forsterite between 790 and 820 °C [50]. Whilst it is commonly reported for forsterite to form above 700 °C under prograde heating, this occurs at much lower temperatures in isothermal studies. Isothermal heating of chrysotile, however, required 30 days at 500 °C to form forsterite [3], 3 h to destroy antigorite at 660 °C [51], and 2 h to dehydroxylate lizardite at 650 °C [52]. In general, isothermal heating of serpentine minerals at 575–600 °C for 12 h results in forsterite formation and, in most cases, in complete destruction of the serpentine structure [53].

It is therefore important to note that, thermal stability determined from prograde heating and isothermal heating is different due to the inverse relationship between decomposition temperature and heating duration. This means that a comparison of thermal decomposition temperatures is applicable only to one type of heating procedure, either prograde or isothermal, but not to both. The results of prograde heating may serve to identify and

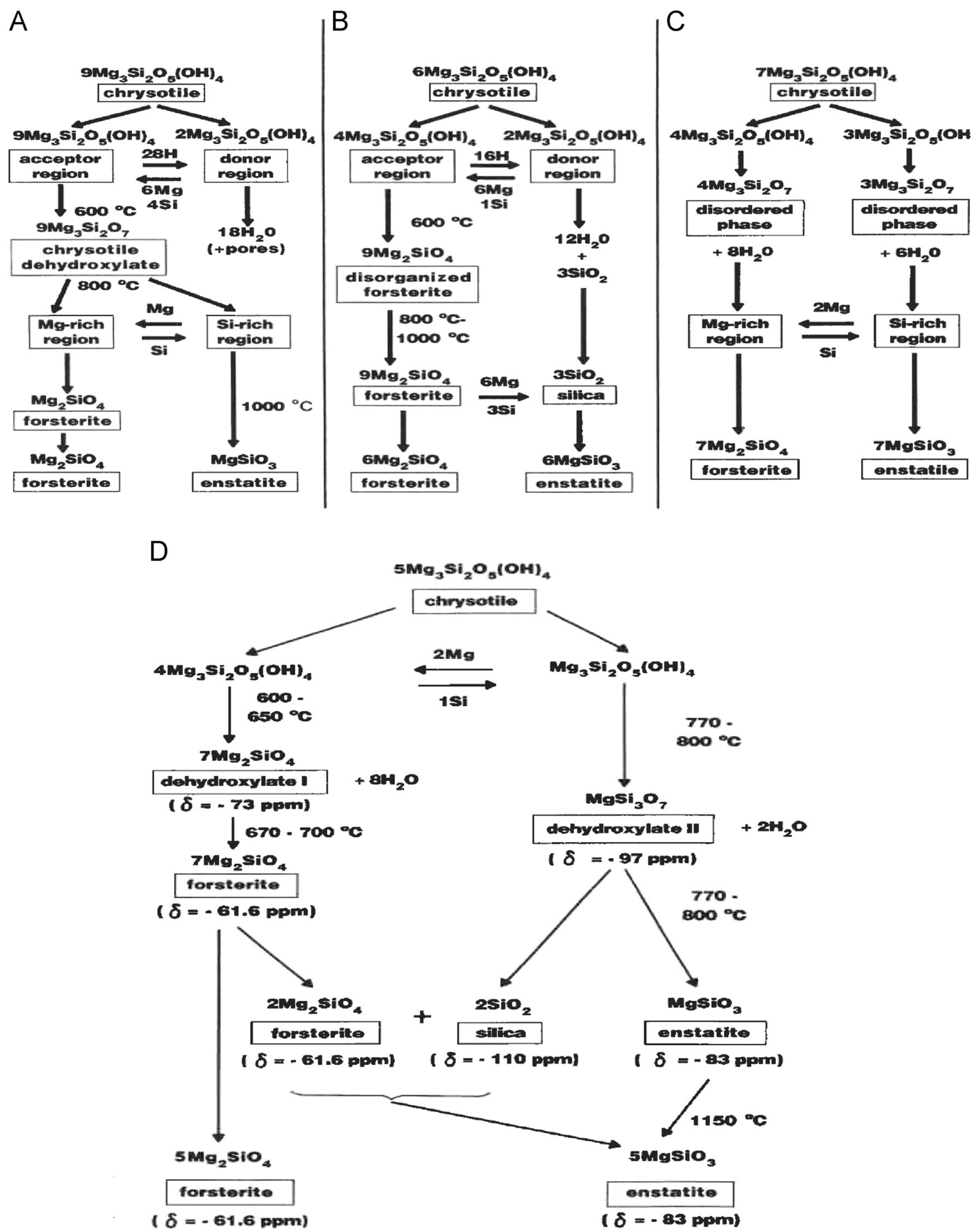


Fig. 3. Proposed thermal reaction sequences for chrysotile [58]. (a) Ball-Taylor 1963, (b) Brindley-Hayami 1965, (c) Martin 1977 and (d) Mackenzie-Meinhold 1994.

quantify serpentine minerals, by correlating the peaks in DTG and DTA/DSC curves with different serpentine minerals and then integrating the areas under the peaks [46,54].

3.2. Thermal reaction sequence

Amongst serpentine minerals, the thermal reaction sequence for chrysotile has been well studied [55–59]. The proposed mechanisms, as shown in Fig. 3, are based on a topotactic transition whereby forsterite and enstatite form from the Mg-rich and Si-rich regions, respectively. Based on their NMR results, MacKenzie and Meinhold [58,60] (Fig. 3d) updated the mechanism of Brindley and Hayami [56] (Fig. 3b) and included the formation of intermediate phases from which forsterite and enstatite nucleate. These mechanisms, however, apply only to thermal treatment under dry conditions ($P_{H2O} \ll 0.1$ Pa) where the relative mobility of tetrahedral layers leads to the formation of forsterite taking on the same orientation as that of the better preserved octahedral layers. This arises from forsterite preferentially forming at the Mg-rich regions (OH-depleted octahedral layer) [55,56,59], where its oxygen (Mg–O) packing resembles the relatively immobile octahedral layer [55]. The mobility of the tetrahedral layer is due to the depolymerisation, reorientation and migration of silica tetrahedra, following water liberation, yielding various silica configurations as sheets, chains and isolated tetrahedra [58].

Under hydrothermal conditions ($P_{H2O} > 32$ bar), the migration of Mg^{2+} from the octahedral layer dictates the pace at which the reaction sequence occurs [55]. (In this review, we follow the definition introduced by Ball and Taylor [55] to designate (1) dry conditions as $P_{H2O} \ll 0.1$ Pa, (2) wet condition, as $P_{H2O} > 0.1$ Pa, and (3) hydrothermal conditions as $P_{H2O} > 32$ bar.) Under this condition, forsterite assimilates the oxygen packing of the silica layer and thus orients itself in similar manner as the tetrahedral layer. In other words, wet conditions induce the disruption of the octahedral layer, whereas dry conditions depolymerise the silica tetrahedra. Whilst dehydroxylation is relatively simpler and faster in dry conditions because liberated water only needs to negotiate the encroaching silica sheets. Under either wet or hydrothermal conditions, the nucleation of forsterite along the tetrahedral layers coupled to increased vapour concentration increase the difficulty with which the liberated water must negotiate its passage through the silica sheets and out of the sample matrix.

The formation of forsterite always precedes enstatite. It is commonly observed that, prograde thermal treatment below 800 °C only forms forsterite. Heating, near or above this temperature for a prolonged period, forms both forsterite and enstatite. Whilst it appears that, forsterite formation does not require full dehydroxylation, the formation of enstatite seemingly does. These apparent temperature dependent reactions are generally expressed in the following equations, respectively:

$$2Mg_3Si_2O_5(OH)_{4(s)} \overset{<800\,^{\circ}C}{\Longrightarrow} 3Mg_2SiO_{4(s)} + SiO_{2(s)} + 4H_2O_{(g)} \quad (1)$$

$$Mg_3Si_2O_5(OH)_{4(s)} \overset{>800\,^{\circ}C}{\Longrightarrow} Mg_2SiO_{4(s)} + MgSiO_{3(s)} + 2H_2O_{(g)} \quad (2)$$

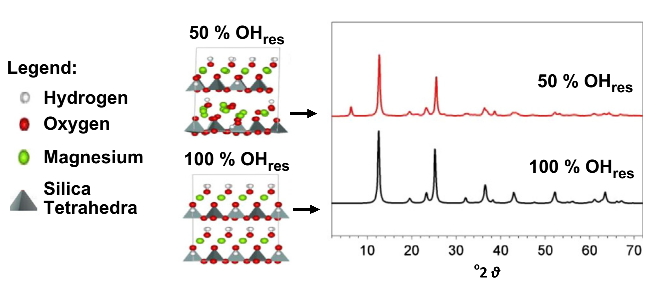


Fig. 4. Structural relaxation of lizardite and its corresponding simulated X-ray diffraction pattern [61]. Removal of the inner layer hydroxyls manifests itself as a low angle ($<10°$ 2θ) reflection [53]. The % OH_{res} denotes the residual hydroxyl content of the mineral; i.e., the bottom (100% OH_{res}) picture corresponds to the initial ordered lizardite structure. Note an imperfect alignment of the silica tetrahedra in the lower plane for 50% OH_{res}.

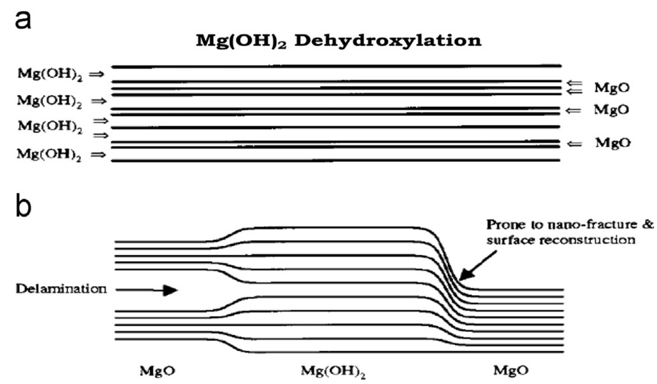


Fig. 5. Lamellar nucleation and growth models for brucite dehydroxylation [64]. Note that, water vapour diffuses sideways, along the same direction as the orientation of the lamellae.

The thermal dehydroxylation of lizardite was studied more recently within the context of mineral carbonation [61]. Based on the results of the theoretical and experimental investigations, researchers proposed that the reaction proceeds via the lamellar dehydroxylation process similar to that exhibited by brucite, where a proton from the cage hydroxyls is liberated first. The cage hydroxyls comprise OH groups wedged between silica tetrahedra, whereas outer hydroxyls are those associated with the octahedral brucite-like layers. At this stage, a charged oxygen atom (previously attached to the departed proton) pries apart two silica tetrahedral inducing the unzippering (i.e., depolymerisation) of the silicate sheet. Whereas, the proton derived from an inner hydroxyl combines with an outer hydroxyl forming a water molecule.

Fig. 4 illustrates the structures of the initial lizardite (100% OH_{res}) and 50% dehydroxylated lizardite (50% OH_{res}) and its respective simulated X-ray diffraction patterns [61]. Simulations indicated that, the removal of the inner hydroxyls results in voids in the lizardite structure. This simulation provides the explanation to the widely observed low angle reflections ($<10°$ 2θ) in the X-ray diffractogram of heat treated serpentine minerals [46,53,62,63]. In essence, the proposed hydroxyl removal sequence of Chizmeshya et al. [61] based on first principles computations provides excellent corroboration of the experimental measurements.

The 50% dehydroxylation constitutes an important value for lizardite. Both theoretical and CO_2 mineralisation studies indicate that carbonation is possible at this value [63]. Beyond 50% dehydroxylation (50% OH_{res}), when all cage hydroxyls have been depleted, protons from the brucite (outer) hydroxyls commence leaving the material. This second stage is more complex due to the entrapment of charged oxygen atoms by the magnesium layers. In addition, the general contraction of the solid structure increases the difficulty of the migration of mobile species. Overall, this two-part mechanism for the thermal dehydroxylation of lizardite parallels that of the thermal sequence of chrysotile.

At a macroscopic level, the dehydroxylation of serpentine is thought to mirror that of brucite, which proceeds either via slow nucleation/rapid growth or rapid nucleation/slow growth processes, as illustrated in Fig. 5 [64]. Slow nucleation/rapid growth favours significant oxyhydroxide intermediate formation whilst rapid nucleation/slow growth preferably forms a two-phase solid (oxide + hydroxide). The treatment temperature influences these

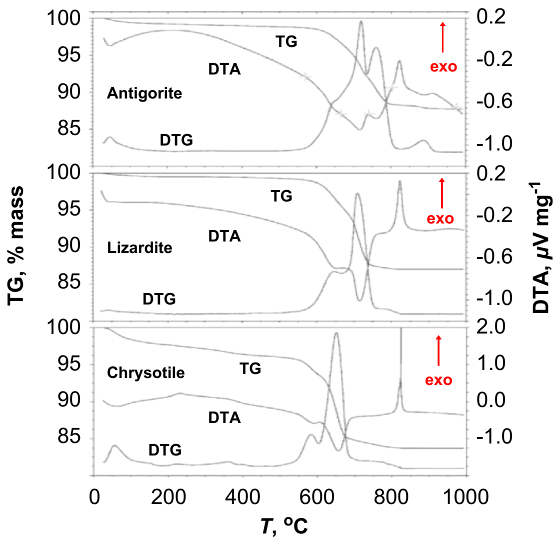


Fig. 6. A typical TGA–DTA curve of antigorite, lizardite and chrysotile [46].

events, whereby higher temperatures favour nucleation whilst lower temperatures the growth process.

3.3. Dehydroxylation products

In broad terms, the thermal dehydroxylation of serpentine reverts the magnesium minerals back to those originally present in peridotite. Even Fe^{3+}, produced initially by oxidation of Fe^{2+}, during the thermal dehydroxylation under air, commences to revert to Fe^{2+} once the temperature reaches 900 °C [65]. The thermal dehydroxylation of serpentine under dry conditions, always forms the same products, forsterite and enstatite [53]. Unlike enstatite, forsterite, however, emerges even prior to full dehydroxylation. The latter forms at temperatures as low as 500 °C, whilst the former only above 800 °C.

The minerals formed during thermal dehydroxylation depend on the heating method used. Generally, forsterite appears at a lower temperature when serpentine undergoes heating at a constant temperature, in comparison to prograde heating; i.e., in heating regime that involves an imposed temperature ramp, usually between 1 and 40 °C min^{-1}. It must be noted, however, that, isothermal treatment requires prolonged heating to achieve full dehydroxylation. For example, isothermal dehydroxylation of chrysotile and lizardite at 500 °C, both under hydrothermal and dry conditions, required 1–7 days to form forsterite [55]. Isothermal dehydroxylation of antigorite at 750 °C also required 20 h to produce forsterite [1]. Whilst the formation temperature of forsterite varies, enstatite only forms above 800 °C, regardless of the heating method. For instance, isothermal treatment of either chrysotile or lizardite for 1–7 days at 1000 °C produced forsterite and enstatite. On the other hand, prograde heating below 800 °C did not yield enstatite [2,46,54]. In general, natural serpentine subjected to either isothermal or prograde heating below 800 °C produces forsterite, whilst the formation of enstatite requires full dehydroxylation and high temperatures above 800 °C [3,51,63].

Whereas isothermal studies rely mostly on X-ray diffraction for identification of mineral phases, prograde studies often employ coupled thermal analytical techniques such as TGA–DTA/DSC to pinpoint the formation temperatures of these products in conjunction with X-ray diffraction. Fig. 6 shows typical TG–DTG–DTA curves of serpentine minerals. In the DTA curve, the dehydroxylation reaction manifests itself as a broad endotherm from 500 to 800 °C, whilst a phase change, which indicates the formation of a new mineral, displays an exotherm centred around 820 °C. The nature of this exotherm is attributed in literature to forsterite formation [48,66], or forsterite recrystallisation [10,51,67], or enstatite formation [46,54]. Some of these studies [46,54,62] identified the formation of crystalline forsterite, by X-ray diffraction, at a much lower temperature (i.e., < 800 °C). Furthermore, a more recent study that collected a complete set of thermal data for serpentine minerals observed that, the exotherm at ∼820 °C coincides with the emergence of the X-ray diffraction pattern for crystalline enstatite [46]. A consensus exists in modern literature that, the exotherm at ∼820 °C corresponds to enstatite and not forsterite formation. A prolonged dehydroxylation endotherm spanning 500–800 °C could mask the formation exotherm of fosterite.

Forsterite and enstatite do not form directly from serpentine, but rather through a topotactic transition involving intermediate phases. Forsterite crystallises from the Mg-rich regions, whilst enstatite from the Si-rich regions of the dehydroxylated serpentine [27]. Thermodilatometric analysis confirmed that forsterite and enstatite emanate from the early matrix of the intermediate "metaserpentine phase" [50]. It was also proposed that dehydroxylation proceeds in a 2-step process, the second stage of which involves the formation of forsterite and enstatite [9].

3.4. Dehydroxylation intermediates

In literature, the transitional phases appear under several names, with their reported stabilities varied depending on the mineralogical composition of a sample [53]. Initially, the term serpentine anhydrite was introduced to denote the dehydroxylated portion of serpentine minerals. Serpentine anhydride phase was described as a chemically damaged solid, characterised by a wide range of activation energies for the formation of forsterite [56]. The intermediates in both chrysotile and antigorite were also labelled as 10+Å phase and talc-like phases [3,9,57]. Concomitant with forsterite formation, a talc-like phase emerges when chrysotile undergoes heating to between 587 and 700 °C [3]. Moreover, a two-step dehydroxylation process, proposed for antigorite, suggests that stage 1 leads to the formation of forsterite and a talc-like phase [9]. All these observations clearly indicate that the topotactic transition of serpentine to forsterite and enstatite involves at least two intermediate phases.

MacKenzie and Meinhold studied these intermediates in more detail using ^{29}Si and ^{25}Mg MAS NMR, to elucidate the thermal reaction sequence of chrysotile [58]. Two intermediate phases were identified and referred to as dehydroxylates I and II. Dehydroxylate I is a Mg-rich phase, characterised by both structural order and disorder. This phase transforms to forsterite at 670–700 °C. Although, this phase retains the original octahedral coordination of the parent mineral, it is X-ray amorphous due to the structural disorder in the tetrahedral layers. On the other hand, dehydroxylate II, is a Si-rich phase that transforms to enstatite and free silica at 770–800 °C. Furthermore, unlike dehydroxylate I where Si sites are disordered and Mg sites are not, Si sites in dehydrohylate II are very similar to crystalline talc with severely disordered Mg sites [58]. Although these dehydroxylates were speculated as chrysotile fibre and not as intermediate phases [3], the evidence suggests that, these are indeed metastable phases [58].

Investigations by Chizmeshya et al., involving advanced computational modelling and experimental measurement by X-ray diffraction and nuclear magnetic resonance, demonstrated that, thermal dehydroxylation of lizardite also proceeds via the formation of intermediates phases [61]. These researchers named two phases, "α" meta-serpentine and amorphous meta-serpentine, to emerge during the early (∼50% dehydroxylation) and late (∼90% dehydroxylation) stages of the reaction, respectively [21,61]. Further investigations on the structure of lizardite undergoing thermal dehydroxylation showed that, the "α" meta-serpentine

phase displayed long-range order. This phase is analogous to the lamellar oxyhydroxide material formed during brucite dehydroxylation [68,69]. In support of experimental measurements, the formation of the "α" metaserpentine has been demonstrated by computational first-principles studies.

It appears that, as the octahedral layer remains immobile, contraction of the mineral structure could be attributed mainly to rearrangements of tetrahedral layers. Solid state Fourier transform infrared (FTIR) spectroscopy revealed that, the local environment of the octahedral layer of brucite remains unchanged during the formation of the "α" metaserpentine phase [63]. A separate study consistently represented a general shrinkage of serpentine structure as function of progress of dehydroxylation [50]. All these manifestations and inferred mobility of the tetrahedral layers are in agreement with the initial observations of Ball and Taylor [55].

Overall, literature presents convincing evidence on the presence of intermediates, in conformity with the topotactic nature of serpentine dehydroxylation. These intermediates are generally designated as anhydride phases, dehydroxylates and metaserpentine phases. In particular, dehydroxylates I and II have been identified for chrysotile whilst "α", and amorphous metaserpentine for lizardite. With respect to thermal dehydroxylation of antigorite, the emergence of the 10+Å and talc-like phases, reported preliminarily in Refs. [5,9], requires further studies.

3.5. Factors influencing thermal dehydroxylation of serpentine

Variations in the kinetic parameters of thermal dehydroxylation of serpentine appears to depend on factors such as particle size, ore purity and crystallinity, processing history (such as vapour pressure of water, purge gas and impact shocking) heating method including thermal cycling, analytical technique and method of kinetic analysis of the measurements [3–5,9,11,45,48,49,55,56,70]. Although no single study covered all these factors, some investigations ascertained in detail the effect and extent of individual parameters.

Several studies pointed out that, particle size significantly influences the peak temperature of dehydroxylation obtained by DTG and DSC/DTA measurements [6,7,45,48,73]. In general, smaller particles exhibited lower dehydroxylation peak temperatures. Although the exotherm at ~810 °C does not change its location significantly, the peak height increases with the decrease in particle size [48]. The ease by which dehydroxylation occurs in smaller particles was attributed to a partially amorphised mineral which resulted from prior mechanical grinding.

It must also be noted that thermal dehydroxylation is affected by matrix introduced with analytical techniques. A combined TGA and FTIR study on the thermal decomposition of chrysotile demonstrated that, the mechanism of transformation of "free" samples differed from that of samples dispersed in a KBr matrix [6]. The subsequent transformation of chrysotile anhydride to forsterite occurred at a much lower temperature (550 °C) for samples dispersed in KBr, whilst the same reaction proceeded at higher temperatures (> 650 °C) for the "free" sample. This marked difference was traced back to the behaviour of tetrahedral layer, as can be seen in the changes in the FTIR spectral intensities of the v_3 Si–O bond. Since serpentine transforms to forsterite topotactically, the rate of crystallisation depends on the degree of structural order. The pressed pellet of chrysotile in KBr media limits the structural distortion upon heating, hence facilitating a relatively earlier onset of formation of forsterite.

The use of a dry and inert purge gas and prograde thermal treatment below the crystallisation temperature of forsterite lowers the peak temperatures of dehydroxylation and maximises structural disorder, respectively. The peak temperature of dehydroxylation of antigorite was lowered by 25 °C (from 775 °C to 750 °C) when nitrogen was used as purge gas instead of air [66]. Although no explanation was provided for the decrease in the temperature of the dehydroxylation peak with the use of non-oxidising purge gas, this phenomenon most likely arises as a consequence of the formation of hematite skins on grains of serpentine that engender mass transfer resistance to the removal of moisture [26]. The possible presence of moisture in the air purge may also provide explanation, as moisture may engender the appearance of a backward reaction.

Thermal treatment below the recrystallisation temperature is a practical and effective method to inflict maximum structural distortion of the mineral structure via the formation of microcracks. Heating of serpentine above its endothermic dehydroxylation peak but below its characteristic exothermic peak temperature renders a highly amorphous solid [44]. This microcrack-laden solid displays reduced thermal conductivity compared to the original mineral. Upon further heating, new crystalline phases form, contracting the material and healing the cracks.

3.6. Reaction kinetics

3.6.1. Kinetic studies

Thermal dehydroxylation of serpentine and its subsequent transformation is a kinetically hindered reaction [12,47,53]. This is evidenced by a 12 h requirement [53] to fully dehydroxylate serpentine minerals and form forsterite when heat treated isothermally near the dehydroxylation equilibrium temperature of about 577 °C [47]. Certainly, at this sluggish rate, production of thermally activated serpentine is neither practical nor economically feasible. Improving the rate at which serpentine dehydroxylates requires employing appropriate strategies that circumvent the rate limiting steps and accelerate the reaction progress. Kinetic studies make available the necessary information, the so-called kinetic triplet, comprising the rate controlling mechanism, the activation energy (E_a) and the pre-exponential factor of water release (A). These kinetic studies are crucial to improving the present understanding of rates of kinetically hindered reactions.

The kinetic parameters of the thermal dehydroxylation of serpentine minerals were previously estimated using a variety of analytical methods and kinetic analyses. Based on DTA experiments performed under wet isobaric conditions ($P_{H2O}=1$ bar), the average reaction order, n, and mean activation energy, E_a, of -44 μm particles of chrysotile, lizardite and antigorite samples were obtained as 0.93 and 399 kJ mol^{-1}, respectively [45]. This indicates that under this condition (small particles, $P_{H2O}=1$ bar), serpentine minerals generally follow the first order reaction mechanism, F1, where nucleation of the new mineral phase is rate-limiting.

A TGA-based study on the thermal treatment of bigger particles of lizardite (177–250 μm) at 630–770 °C under wet isobaric conditions showed the reaction to be limited by a three-dimensional diffusion mechanism in spherical particles, D3, rather than first order kinetics (F1). Furthermore, the E_a was observed to vary from 285 to 502 kJ mol^{-1} when P_{H2O} increased from 0.1 to 6270 Pa [46]. It can be deduced that, serpentine dehydroxylation is influenced by both particle size and vapour pressure of water. Whilst the rate limiting mechanism changes from nucleation (small particles, powdered) to diffusion controlled (bigger particles, crystalline), the presence of water vapour combined to a highly crystalline material can significantly alter the net rate, as water vapour may induce backward reactions slowing down the overall process.

Real-time kinetic studies using in situ XRPD under ambient air conditions were also applied in investigations on thermal dehydroxylation of serpentines. In the dehydroxylation of ~5 μm particles of chrysotile, the rate-limiting mechanism was identified via the Avrami model as the one-dimensional diffusion of water

Table 2
Apparent kinetic parameters (kinetic triplets) for serpentine dehydroxylation as reported in literature.

Mineral	Experimental conditions				Apparent kinetic parameters			Ref.
	Size, μm	T (°C)	P_{H2O} (Pa)	Analytical technique	Reaction model	E_a (kJ mol^{-1})	A (s^{-1})	
Lizardite, Chrysotile, Antigorite	44	25–900	1.0×10^{5}	DTA, β=10 °C min^{-1}	Reaction order, F1	399 ± 126	Not reported	[45]
Lizardite	214	630–770	1.0×10^{-1} to 6.7×10^{3}	TGA	Diffusion, D3	285–502	0.1×10^{1}	[49]
Chrysotile	5	620–750	$<1.0\times10^{-2}$	Real time XRPD, β=75 °C min^{-1}	Avrami–Erofeyev, A	184 ± 8	1×10^{8}	[4]
Antigorite	3	25–800	2.7×10^{9}	Real time XRPD, β=10 °C min^{-1}	Avrami–Erofeyev, A	Not reported	1×10^{-6} to 1×10^{-8}	[9]
Lizardite	83	535–610	1.3×10^{8}	Pore volumetry	Avrami–Erofeyev, A	429 ± 201	Not reported	[70]
Lizardite	20,000	535–610	1.5×10^{8}	Pore volumetry	Avrami–Erofeyev, A	521 ± 22	Not reported	[70]
Antigorite	75	25–1100	$<1.0\times10^{-2}$	TGA, β=10 °C min^{-1}	Geometric contraction, R3	160 ± 7	1×10^{8}	[62]
Antigorite	15	612, 640, 666, 687	$<1.0\times10^{-2}$	Isothermal XRPD	Avrami–Erofeyev, A	255 ± 7	Not reported	[57]
Lizardite	15	625, 638, 642, 645, 666	$<1.0\times10^{-2}$	Isothermal XRPD	Avrami–Erofeyev, A	221 ± 7	Not reported	[57]
Antigorite	98	25–900	$<1.0\times10^{-2}$	TGA, β=100 °C min^{-1}	Geometric contraction, R3	216	6×10^{7}	[71]
Antigorite	328	25–900	$<1.0\times10^{-2}$	TGA, β=100 °C min^{-1}	Geometric contraction, R3	256	3×10^{8}	[71]
Antigorite	463	25–900	$<1.0\times10^{-2}$	TGA, β=100 °C min^{-1}	Geometric contraction, R3	338	9×10^{7}	[71]

molecules, with an apparent activation energy, E_a of 184 kJ mol^{-1} in the temperature range of 620–750 °C [4].

A similar real-time XRPD study on the thermal dehydroxylation kinetics of 3 μm particles of antigorite revealed that the reaction proceeds via a 2-step process and reemphasised a strong influence of H_2O activity on the reaction [9]. Its corresponding kinetic analysis based on the Avrami nucleation model showed that, serpentine dehydroxylation proceeds mainly by surface growth along the edges of the mineral grains [9]. This observation also corroborates results of a similar XRPD study on the dehydroxylation kinetics of ~5 μm particles of antigorite at temperatures of up to 900 °C and at high pressures of 3–9 GPa [5]. The two studies found the nucleation to control the appearance of fosterite, and the growth process to govern the formation of enstatite. These findings provide an explanation for the generally observed decrease in dehydroxylation rate beyond 50% dehydroxylation. For example, the rate of the dehydroxylation reaction of lizardite remains constant between 0% and 50%, decreases slightly from 50% to 80% dehydroxylation, and displays substantial deceleration nearing completion [49,70].

A pore volumetry study demonstrated the differences in the apparent activation energies between crystalline and powdered mineral [70], estimating the activation energies, E_a, for powdered and intact samples of lizardite as 429 ± 201 and 521 ± 52 kJ mol^{-1}, respectively [70]. The powdered samples, besides having a relatively low mean energy barrier, displayed a significant variation in E_a. This variation arises due to the prior size reduction that imparts various degrees of mineral amorphisation and yields a range of structurally distorted material.

Recent studies have identified the activation energy values for dehydroxylation below 700 °C as well as showed the effect of particle size on E_a. Isothermal XRPD on powdered antigorite and lizardite yielded mean E_a values of 255 ± 7 and 221 ± 7 kJ mol^{-1}, respectively [57]. The results indicate that E_a of about 238 kJ mol^{-1} is to be expected for dehydroxylation of small particles (15 μm) of serpentine minerals below 700 °C. Work performed in TGA utilising high heating rate (100 °C min^{-1}) and

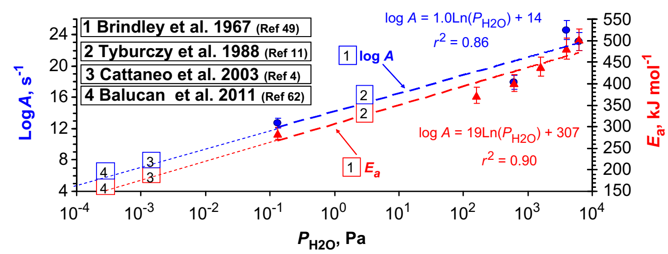


Fig. 7. Vapour pressure (P_{H2O}) dependency of serpentine kinetic parameters E_a and A [4,11,49,62]. Kinetic studies with a complete set of kinetic parameters (boxes 2, 3, and 4) follow the trendlines of the Brindley and Hayami study (box 1).

high purge gas rate (100 L min^{-1}) clearly showed that, the E_a for antigorite dehydroxylation increases with particle size [71].

Table 2 summarises the reported apparent kinetic parameters for thermal dehydroxylation of serpentines. Note that, the derived kinetic parameters assume only a forward reaction but in most cases, the reaction occur under near-equilibrium conditions (i.e., ~577 °C, P_{H2O}~1 bar). Unless P_{H2O} is maintained well below 1.0×10^{-2} Pa, estimates of the activation energy yield apparent values that exceed 200 kJ mol^{-1} with very low A values. The majority of these experimental conditions indicate a non-ideal scenario for the thermal activation of serpentine for mineral carbonation.

Although it is clear from these studies that, the fugacity of water influences the kinetics of serpentine dehydroxylation, inducing the reverse reaction and resulting in the dehydroxylation process to proceed close to equilibrium. The effect of the partial pressure of water is rarely included in kinetic studies [49]. Furthermore, the formation of forsterite and enstatite tends to decelerate the rate of dehydroxylation. It is unclear whether the thermal treatment performed below the crystallisation temperature of either forsterite or enstatite could counteract this deceleration. In addition, isoconversional methodologies [72–74] have not yet been applied in dehydroxylation studies to yield unique estimates of activation energies. It appears that the combination

of these factors provides explanation for significant variation and extremely high E_a values in various studies quoted in Table 2.

3.6.2. Effect of water vapour on reaction kinetics

The partial pressure of water vapour influences serpentine dehydroxylation kinetics, slowing down the liberation of water from the sample matrix. Thermogravimetric experiments involving partial pressure of water vapour ($P_{H2O} > 0.1$ Pa) showed large variations in the rate of dehydroxylation of lizardite [49]. In contrast, a sufficient flow of dry inert purge gas (argon, 20–200 mL min^{-1}) afforded constant kinetic parameters and the lowest measured E_a (160 ± 7 kJ mol^{-1} antigorite) amongst the serpentine dehydroxylation kinetic studies [62]. This highlights that, under dry conditions ($P_{H2O} \ll 0.1$ Pa), kinetic parameters for serpentine dehydroxylation may just be slightly above that of brucite dehydroxylation (E_a = 146 kJ mol^{-1}) [75]. A real-time in situ XRPD study on the mechanism and kinetics of the thermal dehydroxylation of antigorite also revealed strong influence of H_2O activity on the reaction [9]. Elevated pressures (i.e., mechanical compression) do not substantially affect the rate of dehydroxylation reactions, [70] provided that water vapour is removed from above the sample to avoid inducing the reverse reaction. The appearance of reverse reactions makes the dehydroxylation process slow down and proceed closer to the thermodynamic equilibrium [5].

Under dry conditions, the deprotonation of the inner hydroxyls and depolymerisation of the tetrahedral layer primarily control the reaction rate, as these layers serve as a diffusive barrier to migrating water. However, if dehydroxylation takes place under hydrothermal conditions ($P_{H2O} \geq 32$ bar), the controlling mechanism shifts to that of Mg^{2+} migration [52]. The presence or build up of localised $P_{H2O} > 0.1$ Pa may also reduce the rate at which water is liberated. However, if P_{H2O} is considerably larger (≥ 1 bar), the reformation of the octahedral layer may start to predominate.

The work of Brindley and Hayami [49] demonstrated the dependency of serpentine dehydroxylation kinetics on the partial pressure of water vapour. Fig. 7 illustrates this increasing trend in both E_a and A with P_{H2O} (boxes labelled 1 refer to the trendline derived from Brindley and Hayami). Water vapour pressures as low as 0.1 Pa when increased to 1×10^4 Pa result in near doubling of the values of E_a (284–502 kJ mol^{-1}) and A (from log 12.7 to 23.1 s^{-1}). This dependency on P_{H2O} not only highlights the impact of vapour pressure on reaction kinetics but also provides a means to estimate the localised pressure exerted by evolved water within the sample bed. For example, Tyburczy and Ahrens estimated the experimental P_{H2O} in their thermal analysis (boxes labelled 2) using the trend in E_a and A values from the work of Brindley and Hayami [11].

To further explore this concept, we extended the trendlines derived from the work of the Brindley and Hayami (Fig. 7) to include the results of the kinetic studies [4,11,62] that report complete set of E_a and A values (represented as boxes 2, 3 and 4). The plot indicates that, kinetic studies reporting relatively low activation energies, such as those of Cattaneo et al. (E_a = 184 kJ mol^{-1} chrysotile; $A = 1 \times 10^8$ s^{-1}) and Balucan et al. (E_a = 160 kJ mol^{-1}; $A = 1 \times 10^8$ s^{-1} antigorite) are those performed under extremely low P_{H2O}.

It must also be noted that, kinetic studies employing $P_{H2O} \gg 1 \times 10^3$ Pa, [9,45,70] reported E_a values ≥ 400 kJ mol^{-1} and extremely sluggish water release rates, with $A \leq 1 \times 10^{-6}$ s^{-1}. Furthermore, the trend also suggests that for similar thermal studies (Balucan et al., 5 mg powdered sample, flow rate 20 mL min^{-1} argon purge, TGA β = 10 °C min^{-1} versus Tyburczy et al., 20 mg powdered sample, flow rate 20 mL min^{-1} nitrogen purge, DTA β = 10 °C min^{-1} [11,62]) larger sample mass accounts for the larger P_{H2O}.

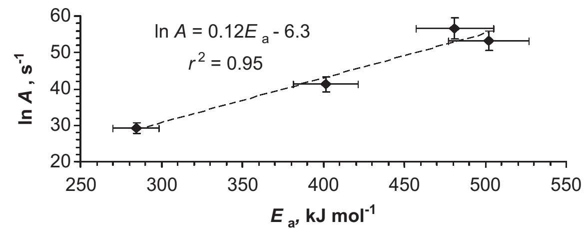


Fig. 8. Relationship between E_a and A of the Brindley and Hayami study depicting the kinetic compensation effect (KCE) [49].

3.6.3. Improving the kinetic data for serpentine dehydroxylation

It is without doubt that, P_{H2O} plays a significant role in dehydroxylation kinetics, and, as such, must be included in the rate equation similar to that developed by Brindley and Hayami [49]. Alternatively, the influence of P_{H2O} may simply be ignored if experimental work is performed under vacuum or under an experimentally determined sufficient flow of purge gas [76]. The latter is only justifiable if the kinetic rates obtained at the strongest possible flow rate of purge gas is the same as those used in the standard kinetic runs [62]. With regards to fundamental kinetic studies, the use of smaller sample mass not only limits the amount of evolved water, improves heat transfer but also minimises the build-up of any localised vapour pressure from entrapped vapour within the sample interstices.

Although the kinetic compensation effect (KCE) [76] may simply be a computational artifact, providing possible reasons to account for this relationship will aid in the overall progress in solid-state kinetics. This commonly observed linear relationship between E_a and A is shown in Eq. (3). The constants a and b correspond to the slope of the line and y-axis intercept, respectively:

$$\ln A = aE_a + b \quad (3)$$

The compensation effect is exemplified in Fig. 8 where kinetic parameters obtained by Brindley and Hayami [49] show a linear relationship. In simple terms, this means that the reaction rate should decrease due to an increase in E_a, an increase in magnitude of ln A "compensates" for such changes. No theoretical explanation has gained general acceptance for this simple relationship.

Modelling the serpentine dehydroxylation kinetics presents numerous challenges, emanating primarily from extending the Arrhenius equation to solid-state kinetics. The innate deficiencies include the validity of the implemented approximations and the failure of current solid-state models to take into account physical factors such as heat and mass transfer and the effect of the gas atmosphere [76]. This means that, complementary techniques and confirmatory studies are necessary to validate both the assumptions and kinetic models. For instance, the kinetic parameters must be tested by means of recreating the experimental data to provide graphical representation of the invoked mechanism.

Second, experiments must employ multiple heating rates to obtain a unique set of kinetic parameters, and treatment of measurements must involve an isoconversional method to obtain a unique evaluation of the activation energy. This approach eliminates the ambiguous determination of the kinetic triplet from a limited set of data, as multiple kinetic models each with different set of kinetic parameters can potentially describe a single TG experiment.

Finally, with the advent of better computing power, non-linear regression (NLR) methods are strongly preferred over the classical linearisation methods. This is because the NLR methods provide a direct means to estimate the kinetic triplet by minimising the deviation between experimental and modelled data. The indirect, conventional linearisation methods, besides relying on an

incomplete expansion of the Taylor expression [62], also distort the Gaussian distribution of errors [76]. Furthermore, direct methods facilitate the fitting of the entire dehydroxylation curve. This enables the identification of appropriate models to either describe the overall thermal sequence or assign best fitting models to certain regions. The former provides best estimates for the overall serpentine kinetics (overall reaction mechanism) whilst the latter affords the identification of rate limiting step (rate controlling step).

4. Mechanical activation by grinding

In general, particle reduction by grinding enhances serpentine dehydroxylation and yields highly disordered material. In addition to accelerated dehydroxylation, the rate of recrystallisation of the reaction products decreases due to the topotactic nature of serpentine transformation [56]. This means that, particle comminution not only enhances the removal of hydroxyls, but it also delays the formation of more structurally rigid forsterite and enstatite. Experiments confirmed that antigorite previously milled then heat treated was structurally disordered, whilst milling after thermal treatment did not afford additional structural disorder [51].

Structural study on the effect of dry grinding of antigorite identified that structural disorder occurred mainly along the *c* axis of the mineral lattice [77]. Consequently, the dehydroxylation reaction was significantly accelerated due to the transformation of structural hydroxyls into adsorbed water in the resulting matrix [7,77]. In addition, the increase in the Si/Mg ratio, obtained from the chemical (AEM, analytical electron microscopy) and structural analysis (FTIR), indicated preferential destruction of the octahedral layers after 10 min of dry grinding. A similar study also showed that grind time of 120 min fully amorphises antigorite due to the complete distortion of the octahedral layers [7]. Mechanical grinding longer than 120 min, however, produced a highly amorphised material with the strong tendency for particle agglomeration [77]. Further grinding to about 240 min completely dehydroxylated antigorite, reducing the structurally bound hydroxyls to mere adsorbed water. Subsequent thermal treatment served to dehydrate the adsorbed water trapped in the solid matrix [7]. It is clear from these studies that, both thermal and mechanical treatment are capable of dehydroxylating serpentine minerals, however, the latter requires additional heating at relatively low temperatures for the complete removal of adsorbed water.

5. Thermomechanical activation

McKelvy et al. have demonstrated the concept of inflicting maximum disorder, without risking particle sintering and, much worse, the recrystallisation to new minerals, in thermomechanical activation studies. They employed mechanical grinding at moderate temperatures using low-level waste heat of ≤250 °C. This type of lizardite activation not only offers carbonation conversions of over 70% [41], but may also provide explanation of the relationship between carbonation and the residual hydroxyls. As can be seen in Fig. 9, the combination of thermal heat at 250 °C and intense ball milling reduced the dehydroxylation temperature, removed ~30% of the hydroxyls as well as increased the crystallisation temperature of reaction products [41]. This provides an excellent evidence of maximising structural distortion via mechanically induced dehydroxylation and concurrent low temperature dehydration.

Fig. 10 illustrates the decreasing trend in the surface area of thermomechanically activated lizardite with increasing temperature. It appears that, whilst grinding with concurrent heating effectively dehydroxylates serpentine, the particles commence to sinter at higher temperature. McKelvy et al. suggested that, because the level of structural disorder appears to be the key

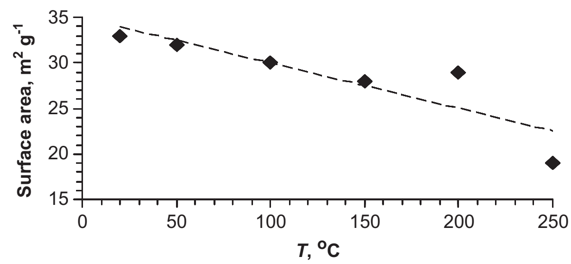


Fig. 10. Measured surface area of the thermomechanically activated lizardite [41]. The temperature at which the grinding was performed is plotted on the *x*-axis.

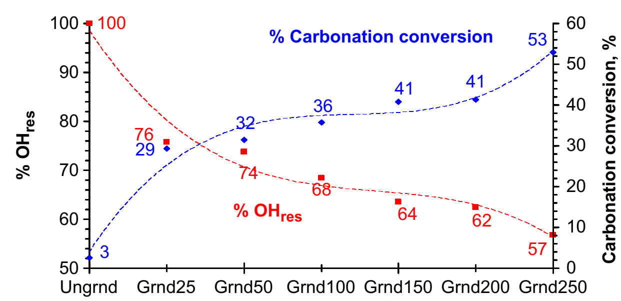


Fig. 11. The effect of temperature on the dehydroxylation and subsequent carbonation of thermomechanically activated serpentine. The numbers after the "Grnd" (i.e., Grnd25 for grounded at 25 °C) denote the operating temperature at which grinding was performed. Note that, the extent of dehydroxylation corresponds closely to the extent of carbonation. Measurements taken from McKelvy et al. [41]. Carbonation of the thermomechanically activated samples was performed at 155 °C, 150 bar P_{CO_2} for 1 h in an aqueous solution comprising 0.64 M $NaHCO_3$ and 1.0 M NaCl.

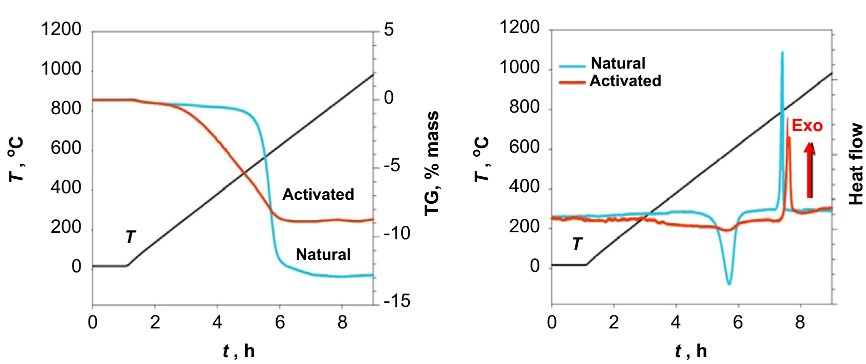


Fig. 9. The TGA–DSC curves of natural and thermomechanically activated lizardite [41].

factor in enhancing carbonation reactivity, addition of high grade heat (in excess of 250 °C) in thermomechanical grinding may decrease the carbonation reactivity due to further reduction of surface area [41]. This means that only low grade heat ($<$ 250 °C) in conjunction with mechanical grinding may serve as an alternate to high temperature heat activation.

The combination of mechanically induced amorphisation and simultaneous thermal dehydration could indeed be a promising method for the activation of serpentine. It is important to note that, at this low temperature activation, the crystallisation of forsterite and enstatite appears to be either minimised or inhibited. Fig. 11 illustrates the relationship between the % OH_{res} and % carbonation conversion as function of grinding temperature. It shows that with thermomechanical activation, the amount of removed hydroxyls (24–53% OH_{res}) corresponds remarkably to the % carbonation conversion. Grinding alone removes ~24% of the hydroxyls, leading to subsequent 26% carbonation. Grinding with concomitant heating to drive off water removed between 26% and 53% of the lizardite's original hydroxyl content, depending on the treatment temperature. The corresponding carbonation conversions between 29% and 50% match closely the amount of removed hydroxyls. This clearly suggests that, the extent of carbonation corresponds to the amount of removed hydroxyls, provided that particle sintering and recrystallisation are avoided. Unlike high temperature treatment ($>$ 600 °C), where carbonation requires serpentine containing only 15–50% OH_{res}, thermomechanical treatment can induce carbonation of serpentines characterised by more than 50% OH_{res}.

6. Shock activation

A study on impact shocking of serpentines found that, for shocked minerals, the dehydroxylation reactions occur at temperature of between 50 and 70 °C below that of unshocked samples [11]. Powdered samples confined in a stainless steel chamber were pressed with a containing plug up to 35 GPa. Shock pressures from 23 to 35 GPa reduced the DSC-derived apparent activation energy, E_a, from 340 ± 15 kJ mol^{-1} to 220 ± 11 kJ mol^{-1} for the unshocked and shocked serpentine, respectively, with the pre-exponential factor decreasing from $10^{12.7}$ to $10^{10.3}$. This means that at 600 °C, shocking accelerates subsequent dehydroxylation by 24 times. The application of the work was to elucidate whether planetary impacts into serpentine rocks, at relatively low temperatures of around −90 °C, have potential to dehydrate serpentine. At this temperature, the impact shocking increases the dehydroxylation rate by 20–30 orders of magnitude, although the absolute rates are miniscule in the order of 10^{-52} s^{-1}. Unfortunately, the study was not performed for mineral carbonation, and did not carry out carbonation reaction to assess an effect on reactivity of shocked ultramafics. As the study provided no XRD evidence of structural disorder stimulated by impact shocking, and there exists no practical implementation of the method to processing large quantities of rocks, the application of impact shocking to activate serpentinites remains an outstanding research question.

7. Activation assisted by sonication

Ultrasonic treatment for between 10 and 250 h lowered the DTG and DTA dehydroxylation peak temperatures by between 5 and 32 °C. This slight improvement despite extended duration is primarily due to the alteration of serpentine texture without imparting significant structural damage to the mineral structure [67]. Further studies confirmed that, particle reduction by sonication merely disengages agglomerated particles, without necessarily destroying the mineral structure [78]. Sonication does not break chemical bonds; it merely induces a more efficient release of liberated water during thermal treatment. This is because the declustered particles afford better mobility of the water molecules as they exit through the powdered matrix.

8. Energy requirements

As shown in Eq. (4), the total thermal energy, Q_{total}, required to dehydroxylate serpentine minerals comprises both sensible, $Q_{sensible}$, and latent heat, Q_{latent}, which must be supplied to the material. Sensible heat refers to the heat required to raise the temperature of the material to the desired treatment temperature. Its value is calculated by integrating the heat capacity, C_p, over a desired temperature range. This is shown in Eq. (5), where m and ΔT correspond to the mass of material and the required increase in temperature, respectively, and C_p^{aver} to the average heat capacity in the temperature range. It must be noted however that serpentine minerals rarely occur as pure chemical species but as serpentinite ores. As such, approximations based on the theoretical calculations may underestimate the actual requirement of sensible heat.

Latent heat corresponds to the combined enthalpy of the dehydroxylation and recrystallisation. This is because forsterite formation occurs during the ongoing dehydroxylation. Simple thermodynamic calculations based solely on water removal that neglect the forsterite formation could overestimate the real requirement for latent heat. This is because the crystallisation of forsterite is exothermic, and may provide a portion of the necessary heat for an on-going endothermic dehydroxylation reaction. Furthermore, as accessory minerals such as carbonates, other silicates, magnetite and organics contribute to the total energy requirement, measured values provide a more accurate dataset than theoretical approximations:

$$Q_{total} = Q_{sensible} + Q_{latent} \tag{4}$$

$$Q_{sensible} = mC_p^{aver}\Delta T \tag{5}$$

$$Q_{latent} \approx \Delta H_{dehydroxylation} \tag{6}$$

The enthalpy of dehydroxylation, $\Delta H_{dehydroxylation}$, for antigorite, chrysotile and lizardite had been previously determined as 367, 414 and 565 kJ kg^{-1}, respectively [45]. Although it appears that, antigorite exhibits the lowest dehydroxylation enthalpy, it displays the highest dehydroxylation temperature amongst these minerals. The observed dehydroxylation peak temperatures for antigorite, chrysotile and lizardite are 700, 664 and 635 °C, respectively [45]. This means that, if thermal treatments are conducted at their respective characteristic peak temperatures, the sensible heat required for antigorite exceeds that necessary for either chrysotile or lizardite. In general, the enthalpy values correlate inversely with the DTG peak temperature, T_P, and nickel content [45].

The total energy requirement for the thermal dehydroxylation of antigorite and lizardite at 630 °C was calculated based on the previously measured heat capacity, C_p, of antigorite (at 120–575 °C), [8] and added to the measured $\Delta H_{dehydroxylation}$ values of 95 and 131 kJ mol^{-1} for antigorite and lizardite, respectively [79]. The estimated total energy requirement for thermal treatment at 630 °C for antigorite and lizardite amounts to 1163 and 1292 kJ kg^{-1}, respectively. This includes $Q_{sensible}$ of 817 kJ kg^{-1}for heating from 25 to 630 °C and Q_{latent} of 346 kJ kg^{-1} for antigorite and 475 kJ kg^{-1} for lizardite [21,80].

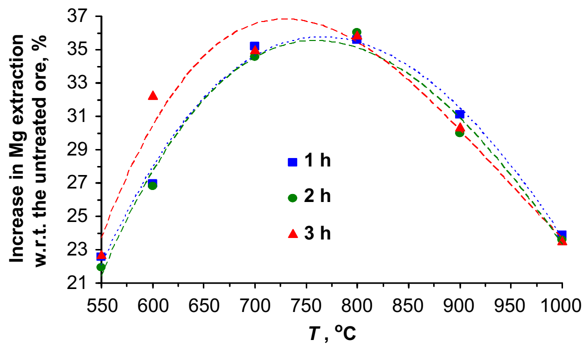


Fig. 12. Enhancements in the extraction of Mg from antigorite with respect to the activation temperature [83].

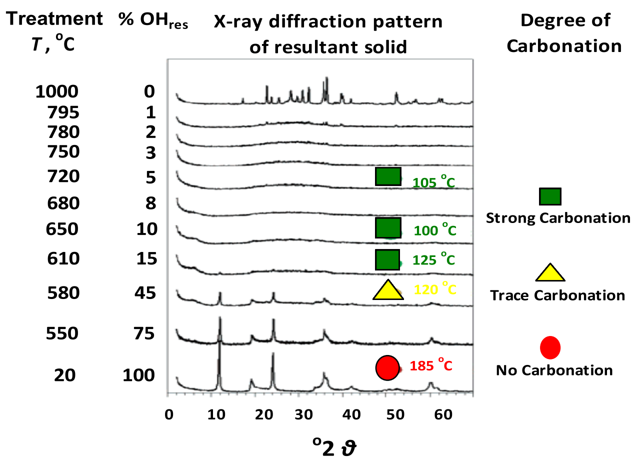


Fig. 13. Degree of carbonation with respect to the % residual hydroxyl content, % OH_{res} of lizardite [63]. The onset carbonation temperatures are placed beside the symbols denoting the extent of carbonation. Carbonation was performed using P_{CO2} = 150 bar and in an aqueous solution of 0.64 M $NaHCO_3$ + 1.0 M NaCl.

9. Magnesium extraction and carbonation efficiency

In the context of direct aqueous mineral carbonation, thermal treatment of serpentine serves to increase magnesium availability for reaction with CO_2. As the rates of dissolution for natural crystalline magnesium silicates increase according to order enstatite < serpentine < forsterite, it is best to avoid overheating to inhibit the formation of enstatite. Recent studies observed significantly enhanced levels of Mg extraction by leaching with acids when serpentinites are thermally conditioned. Heat-treated lizardite between 640 and 700 °C for about 1 h yielded 30% more Mg when leached by HCl as compared to either the natural ore or overheated sample (720–800 °C) [81]. Recently, our group found that, as much as 66% Mg of the total magnesium content can be extracted by a weak acid (formic acid) from a heat-treated (720 °C) antigorite containing 36% OH_{res} [82]. Both these studies show that an optimum degree of dehydroxylation is necessary to maximise the effect of thermal treatment.

Antigorite roasted to between 550–1000 °C for 1–3 h prior to leaching with sulphuric acid demonstrated considerable enhancement in the extraction yields [83]. Fig. 12 illustrates the increase in efficiency in Mg extraction by as much as 36% at between 700 and 800 °C.

The numerous studies by the Albany Research Center (ARC, now part of the US National Energy Technology Laboratory) on thermal activation of lizardite and antigorite reaffirm that protracted heating is counterproductive. Heat treatment above 650 °C to remove the remaining 1–2% hydroxyls proved inefficient [44]. Activation at temperatures above 650 °C under CO_2 atmosphere did not improve the extent of carbonation [52]. In general, whilst isothermally treating antigorite below 600 °C for 2 h is ineffective, heating above 650 °C for the same duration may be counterproductive [84].

Other researchers found that, heat activation of antigorite at 650 °C using steam (unspecified duration) and at 630 °C under air atmosphere for 3 h were successful in increasing antigorite's surface area from 8.2 $m^2\,g^{-1}$ to 15.8 and 17.3 $m^2\,g^{-1}$, respectively [85]. However, only the steam-activated sample was carbonated reaching 60% conversion. Whilst the resultant material for the steam-activated sample was mostly forsterite, unfortunately, no X-ray diffraction pattern was shown for the air-activated sample. It is very likely, however, that prolonged heating in air (dry conditions, 3 h) had transformed antigorite to enstatite, rendering it extremely hard to carbonate.

The Albany Research Center reported the best-case carbonation conversion for heat activated serpentine (heat treatment at 630 °C for 2 h) of 92% and 40% for antigorite and lizardite, respectively [21,86]. Further in situ synchrotron X-ray diffraction investigations revealed that, the degree of carbonation varies with the residual hydroxyl content, % OH_{res}. These studies suggest that, the onset of carbonation was closely associated with the metaserpentine intermediate [63]. Fig. 13 shows that, lizardite containing 45% OH_{res} readily carbonates at 120 °C. Simulations of dehydroxylated lizardite structure pointed out that, the metaserpentine presence was strongest at about 50% dehydroxylation, concurring with the onset of carbonation [61]. As seen in Fig. 13, lizardite with 5–15% OH_{res} sample exhibited strong carbonation at significantly lower temperatures (100–125 °C). Unfortunately, only four of the heat-treated samples between 5% OH_{res} and 45% OH_{res} were examined. Hence, it is yet unclear whether carbonation occurs for samples with < 5% OH_{res}.

A more recent work, involving a wider range of dehydroxylated material from 0% OH_{res} to 100% OH_{res}, gives indication of the optimal degree of dehydroxylation [87]. In this study, heat-treated lizardite was dissolved in acid to extract magnesium. The leachate was subsequently alkalised and then carbonated using simulated flue gas until neutral pH. This solution was then heated to 80 °C for 15 min after which the precipitates were collected. Fig. 14 indicates the reaction extent of over 85% for both dissolution and carbonation of heat-treated lizardite containing between 8% OH_{res} and 25% OH_{res}. In particular, heat-treated lizardite with 16% OH_{res} displayed remarkable dissolution and carbonation behaviour reaching 99% and 97% conversion, respectively. It is also evident that, the fully dehydroxylated lizardite (0% OH_{res}) was inferior to the partially dehydroxylated mineral with 16 ± 8% OH_{res}. Based on

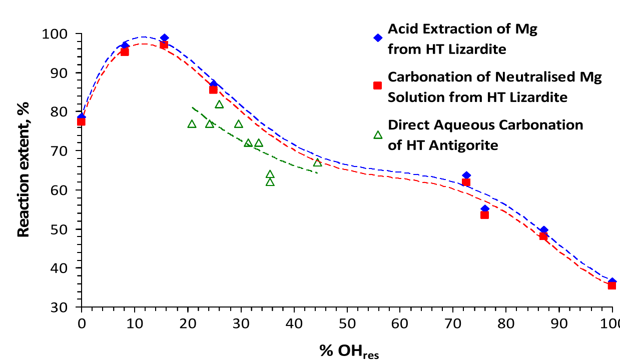


Fig. 14. The extent dissolution and carbonation reaction for heat-treated lizardite [87] and the extent of carbonation reaction of heat-treated antigorite [77] at various degree of dehydroxylation, % OH_{res}. Lizardite carbonation was performed by introducing simulated flue gas into the alkalised leachate until neutral pH, after which, the solution was heated to 85 °C for 15 min. Antigorite carbonation was performed at > 155 °C using P_{CO2} ~ 150 bar and in an aqueous solution of 0.64 M $NaHCO_3$ + 1.0 M NaCl. HT = heat activated.

Table 3
Summary of the carbonation conversions as a function of the degree of dehydroxylation, % OH_{res}.

Mineral	Degree of dehydroxylation (% OH_{res})		Degree of carbonation (% conversion)		Ref.
	Studied range	Optimal	Carbonation conditions	Carbonation conversion	
Lizardite	5–45	10 ± 5 (Fig. 13)	150 bar P_{CO2}, 100 °C onset of carbonation	Strong (numerical value not reported)	[63]
Lizardite	0–100	16 ± 8 (Fig. 14)	Alkalised leachate neutralised with CO_2 and heated 85 °C for 15 min	95	[87]
Antigorite	20–45	< 30 (Fig. 14)	150 °C, 150 bar P_{CO2}, 1 h	82	[84]

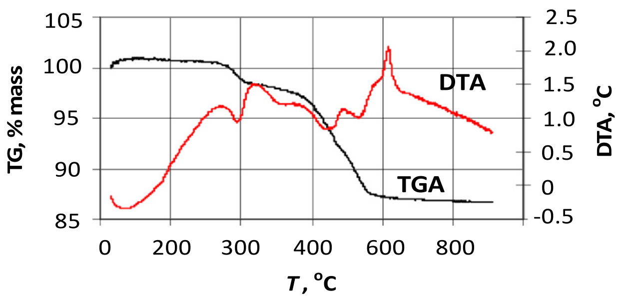


Fig. 15. The TGA–DTA curve of antigorite sample which had achieved 92% carbonation conversion [88]. The first weight loss of about 2.5% at ~400 °C is attributed to the dehydroxylation of brucite.

this result, full dehydroxylation is therefore not only unnecessary, but it is also counter-productive.

The ARC studies on antigorite also noted that, variations in the LOI values (loss on ignition at 1000 °C) of the heat-treated material seemingly dictated the extent of carbonation [84]. These LOI values correspond roughly to the residual hydroxyl content, % OH_{res}. Fig. 14 shows the extent of carbonation for antigorite containing between 20% OH_{res} and 45% OH_{res}. As can be seen, heat-treated antigorite containing < 34% OH_{res} obtained carbonation conversions over 70%. The similarity in the trends in Fig. 14 indicates that, the dehydroxylated form of both lizardite and antigorite possess similar reactivity. Their difference in the extent of carbonation is simply due to the relative ease of carbonating an alkalised leachate of heat-treated lizardite as compared to the direct aqueous carbonation of a powdered solid of heat-treated antigorite.

The reactivity of heat-treated serpentine at various degree of dehydroxylation is evident in the dissolution trend (acid extraction) in Fig. 14. This trend is independent of the carbonation conditions and provides a direct measure of the enhancement in Mg availability as a function of to the degree of dehydroxylation. This indicates that 16 ± 8% OH_{res} is the optimal degree of dehydroxylation of lizardite. If Mg is readily available, carbonation conversion follows that of the dissolution trend. Since both the heat treated antigorite and lizardite depict similar trends, antigorite, at this degree of dehydroxylation, is also expected to depict similar reactivity. It is therefore highly recommended that thermal treatment of serpentine minerals target the optimal degree of dehydroxylation corresponding to 16 ± 8% OH_{res}.

Table 3 summarises the carbonation conversions for heat-treated serpentines, together with % OH_{res} reported in literature. Based on the carbonation results, unless the heat-treated mineral undergoes prior acid leaching and its leachate is subsequently alkalised, only solids with < 50% OH_{res} readily carbonate. Whilst the carbonation-active minerals would contain between 0% OH_{res} and 50% OH_{res}, only those comprising between 5% OH_{res} and 20% OH_{res} could reach > 90% conversions in either dissolution or carbonation.

The significant difference in carbonation conversion between antigorite (92%) and lizardite (40%) in the ARC studies was first attributed to brucite. Fig. 15 shows the weight loss of ~2.5% from 375 to 420 °C to correspond to this brucite component. Although the brucite component (~19%$_{w/w}$) readily carbonates and could increase the carbonation yield, the increase could not match the considerable disparity between the lizardite and antigorite [88]. The differences in thermal stability between lizardite and antigorite, however, suggest that, activation at 630 °C for 2 h may have fully dehydroxylated lizardite and induced the crystallisation of forsterite and possibly enstatite. On the contrary, antigorite which has higher thermal stability than lizardite, could have only been partially dehydroxylated to render a structurally disordered solid without inducing forsterite or much worse, enstatite crystallisation. As serpentine dehydroxylation undergoes a topotactic transformation, structural distortion must be maximised to produce a carbonation-active material.

10. Heat treatment processes

The current energy estimates for the direct aqueous carbonation of thermally activated serpentine were reported in terms of electrical energy (kWh_e), indicating the use of electricity for serpentine activation [21]. The use of electrical energy for serpentine activation is not only inefficient but also impractical, resulting in CO_2 emissions from them exceeding the CO_2 sequestered. Direct use of thermal heat is necessary for serpentine activation.

Various patents describe direct application of thermal energy for heat treatment of serpentine. For example, the pulvurised silicate can be subjected to an upward rising turbulent hot gas [89]. This configuration in essence corresponds to a fluidised bed reactor. In a recent patent, thermal heat generated from combustion of carbonaceous or hydrocarbonaceous fuels combined with ≥ 20% renewable biomass was proposed as this entails much less CO_2 emissions than the combustion of coal [90]. Another patent described the direct use of thermal heat with hot synthesis gas from coal gasification to thermally activate serpentine minerals in a fluidised bed reactor [91]. Whilst alternate fuel sources were considered, an efficient heat treatment may need to involve process heat integration and thermal recycling to further reduce the energy requirements [92]. Rapid heating or thermal shocking of serpentine as described in another patent aimed to simplify the activation process and to reduce its duration [93]. Overall, this requires the development of effective thermal activation equipment with heat recovery.

11. Conclusion

This paper reviewed the studies on dehydroxylation of serpentine minerals, focussing on applications of dehydroxylation for CO_2 mineralisation. We evaluated, and wherever possible quantified, the thermal stability, thermal dehydroxylation sequence, product and intermediate phase formation, factors that influence the dehydroxylation process, kinetics and mechanisms, associated energy estimates, and the dissolution and carbonation efficiencies.

Structural disorder constitutes the primary factor controlling the availability of magnesium for either extraction or carbonation. Reaction kinetics and the governing mechanisms are highly dependent on the activity of water and recrystallisation of product phases.

The reaction mechanism involves structural reorganisation that comprises nucleation and growth of new mineral phases. Thermal activation must be operated in such a manner that, P_{H20}, recrystallisation of the structure and particle sintering are either minimised or eliminated. The transition from serpentine to forsterite and enstatite follows a topotactic transformation, in which the rate decreases with increasing degree of disorder. This means that, amorphisation must involve no or little recrystallisation, especially, no formation of enstatite. The order of reactivity of carbonation reactions corresponds to disordered serpentine > forsterite > serpentine > enstatite.

In summary, evidence suggests that, structural disorder plays a dominant role in the dissolution and carbonation efficiencies of thermally treated serpentine. Serpentines, once devoid of the structurally bound water, must be prevented from regaining structural order through careful consideration of the treatment temperature to avoid overheating.

In light of this review, prior energy approximations do not always reflect the necessary energy requirement. This is because more reactive serpentines do not require full dehydroxylation, whilst prior energy estimates considered the latent heat for full dehydroxylation coupled to theoretical estimates of sensible heat. Actual energy measurements are therefore necessary to provide realistic energy estimates.

Acknowledgements

Reydick Balucan thanks The University of Newcastle for the postgraduate research scholarships. We are grateful to Professors Eric Kennedy and John Mackie of the University of Newcastle, Australia, for their comments and advice.

References

[1] Aruja E. An X-ray study of the crystal structure of antigorite. Miner Mag 1945;27:65–74.
[2] Hargreaves A, Taylor WH. An X-ray examination of the decomposition of chrysotile and serpentine. Miner Mag 1946;27:204–16.
[3] Candela PA, Crummett CD, Earnest DJ, Frank MR, Wylie AG. Low pressure decomposition of chrysotile as a function of time and temperature. Am Miner 2007;92:1704–13.
[4] Cattaneo A, Gualtieri AF, Artioli G. Kinetic study of the dehydroxylation of chrysotile asbestos with temperature by in-situ XRPD. Phys Chem Miner 2003;30:177–83.
[5] Inque T, Yoshimi I, Yamada A, Kikegawa TJ. Time-resolved X-ray diffraction analysis of the experimental dehydration of serpentine at high pressure. J Miner Petrol Sci 2009;104:105–9.
[6] Jolicoeur C, Duchesne D. Infrared and thermogravimetric studies of the thermal degradation of chrysotile asbestos fibers: evidence for matrix effects. Can J Chem 1981;59:1521–6.
[7] Kim DJ, Chung HS. Effect of grinding on the structure and chemical extraction of metals from serpentine. Part Sci Technol 2002;20(2):159–68.
[8] King EG, Barany R, Weller WW, Pankratz LB. Thermodynamic properties of forsterite and serpentine. United State Department of Interior, Bureau of Mine; 1967.
[9] Perrillat JP, Daniel I, Koga KT, Reynard B, Cardon H, Crichton WA. Kinetics of antigorite dehydration: a real-time x-ray diffraction study. Earth Planet Sci Lett 2005;236:899–913.
[10] Rao VAN, Murty MS. Thermal studies on soft and brittle asbestos. Curr Sci 1979;48:760–1.
[11] Tyburczy JA, Ahrens TJ, Dehydration kinetics of shocked serpentine. In: Proceedings of the 18th lunar and planetary science conference, Houston, Texas, March 16–20, 1987. Houston, Texas; 1988.
[12] Faust GT, Fahey JJ. The serpentine group minerals. U.S. Geol Surv Prof Pap 1962;384-A:92.
[13] Page NJ. Chemical differences among the serpentine "polymorphs". Am Miner 1968;53:201–15.
[14] Metz B, Davidson O, de Coninck HC, Loos M, Meyer LA, editors. IPCC. Special report on carbon capture and storage. Cambridge, UK: Cambridge University Press; 2005.
[15] Goff F, Guthrie GD, Lipin B, Fite M, Chipera SJ, Counce D, et al. Evaluation of ultramafic deposits in the eastern United States and Puerto Rico as sources of magnesium for carbon dioxide sequestration. Los Alamos, New Mexico: Los Alamos National Laboratory; 2000.
[16] Huijen WJJ, Comans RNJ. Carbon dioxide sequestration by mineral carbonation: literature review, ECN-C-05-022. The Netherlands: Energy Research Centre of the Netherlands; 2005.
[17] Huijen WJJ, Comans RNJ. Carbon dioxide sequestration by mineral carbonation: literature review, ECN-C-03-016. The Netherlands: Energy Research Centre of the Netherlands; 2003.
[18] IEAGHG. CO_2 storage as carbonate minerals. PH3/17. Cheltenham, United Kingdom: CSMA Consultants Ltd; 2000.
[19] Sipila J, Teir S, Zevenhoven R. Carbon dioxide sequestration by mineral carbonation-Literature review update. Report VT 2008-1. Turku, Finland: Abo Akademi University, Heat Engineering Laboratory; 2008 ⟨http://web.abo.fi/~rzevenho/MineralCarbonationLiteratureReview05-07.pdf⟩ [accessed July 2009].
[20] Budzianowski WM. Value-added carbon management technologies for low CO2 intensive carbon-based energy vectors. Energy 2012;41:280–97.
[21] Gerdemann SJ, O'Connor WK, Dahlin DC, Penner LR, Rush H. Ex-situ aqueous mineral carbonation. Environ Sci Technol 2007;41(7):2587–93.
[22] Khoo HH, Tan RBH. Life cycle evaluation of CO_2 recovery and mineral sequestration alternatives. Environ Prog 2006;25(3):208–17.
[23] Rayson M, Magill M, Sault R, Ryan G, Swanson M. Mineral sequestration of CO_2. Australia: The University of Newcastle; 2008.
[24] Huijen WJJ, Ruijg GJ, Comans RNJ, Witkamp GJ. Energy consumption and net CO_2 sequestration of aqueous mineral carbonation. Ind Eng Chem Res 2006;45:9184–94.
[25] Balucan RD, Dlugogorski BZ, Kennedy EM, Belova IV, Murch GE. Energy cost of heat activating serpentinites for CO_2 storage by mineralisation. Int J Greenh Gas Control 2013;17:225–39.
[26] Balucan RD, Dlugogorski BZ. Thermal activation of antigorite for mineralisation of CO2. Environ Sci Technol 2013;47:182–90.
[27] Burzo E. Serpentines and related silicates. Phyllosilicates. Berlin, Heidelberg: Springer-Verlag; 2009 (col. 27I5b).
[28] Moody JB. Serpentinization: a review. Lithos 1976;9:125–38.
[29] O'Hanley DS, Wicks F. Conditions of formation of lizardite, chrysotile and antigorite, Cassiar, British Columbia. Can Miner 1995;33:753–73.
[30] Wicks FJ, O'Hanley DS. Serpentine minerals: structures and petrology. Rev Miner Geochem 1988;19:91–167.
[31] Evans BW. The serpentinite multisystem revisited: chrysotile is metastable. Int Geol Rev 2004;46:479–506.
[32] O'Hanley DS. Serpentinites: records of tectonic and petrological history. Oxford, United Kingdom: Oxford University Press; 1996.
[33] Whittaker EJW, Zussman J. The characterisation of serpentine minerals by X-ray diffraction. Miner Mag 1956;31:107–26.
[34] Whittaker EJW, Zussman J. The characterization of serpentine minerals. Am Mineral 1958;43:917–20.
[35] Evans BW. Lizardite versus antigorite serpentinite: magnetite, hydrogen and life. Geology 2010;38:879–82.
[36] O'Hanley DS, Dyar MD. The composition of lizardite 1 T and the formation of magnetite in serpentinites. Am Miner 1993;78:391–404.
[37] Uehara S, Shirozu H. Variations in chemical composition and structural properties of antigorites. Miner J 1985;12:299–318.
[38] Uehara S. TEM and XRD study of antigorite superstructures. Can Miner 1998;36:1595–605.
[39] Wunder B, Baronnet A, Schreyer W. Ab-initio synthesis and TEM confirmation of antigorite in the system $MgO–SiO_2–H_2O$. Am Miner 1997;82:760–4.
[40] Wunder B, Wirth R, Gottschalk M. Antigorite: pressure and temperature dependence of polysomatism and water content. Eur J Miner 2001;13:485–95.
[41] McKelvy MJ, Diefenbacher J, Nunez R, Carpenter RW, Chizmeshya AVG. Simultaneous mechanical and heat activation: a new route to enhance serpentine carbonation reactivity and lower CO_2 mineral sequestration process cost. Tempe, AZ: Arizona State University; 2005; 21.
[42] Frost BR, Beard JS. On silica activity and serpentinization. J Petrol 2007;0:1–18.
[43] Luce RW, Bartlett RW, Parks GA. Dissolution kinetics of magnesium silicates. Geochim Cosmochim Acta 1972;36:35–50.
[44] O'Connor W, Dahlin DC, Nilsen RP, Rush GE, Walters RP, Turner PC. CO_2 storage in solid form: a study of direct mineral carbonation. In: 5th International conference on greenhouse gas technologies, DOE/ARC-2000-01. Cairns, Australia, Cairns, Australia; August 14–18, 2000.
[45] Weber JN, Greer RT. Dehydration of serpentine: heat of reaction and reaction kinetics at $P_{H2O}=1$ atm. Am Miner 1965;50:450–64.
[46] Viti C. Serpentine minerals discrimination by thermal analysis. Am Miner 2010;95:631–8.
[47] Seipold U, Schilling FR. Heat transport in serpentinites. Tectonophysics 2003;370:147–62.
[48] Martinez E. The effect of particle size on the thermal properties of serpentine minerals. Am Miner 1961;46:901–12.
[49] Brindley GW, Narahari A, Sharp JH. Kinetics and mechanism of dehydroxylation processes: II. Temperature and vapor pressure dependence of dehydroxylation of serpentinite. Am Miner 1967;52:1697–705.
[50] Ashimov UB, Bolotov YA, Arykbaev RK, Shipkov NV. Thermal analysis of serpentinites. Refract Ind Ceram 1989;30:491–4.
[51] Hršak D, Sučik G, Lazić L. The thermophysical properties of serpentinite. Metalurgija 2008;47:29–31.
[52] Dahlin DC, O'Connor WK, Nilsen RP, Rush GE, Walters RP, Turner PC. A method for permanent CO_2 mineral carbonation. In: 17th Annual international Pittsburg coal conference, DOE/ARC-2000-012. Pittsburgh, PA; September 11–15, 2000.

[53] Brindley GW, Zussman J. A structural study of the thermal transformation of serpentine minerals to forsterite. Am Miner 1957;42:461–74.
[54] Viti C, Giacobbe C, Gualtieri AF. Quantitative determination of chrysotile in massive serpentinites using DTA: implications for asbestos determinations. Am Miner 2011;96:1003–11.
[55] Ball MC, Taylor HFW. The dehydration of chrysotile in air and under hydrothermal conditions. Miner Mag 1963;33:467–82.
[56] Brindley GW, Hayami R. Kinetics and mechanisms of dehydration and recrystallization of serpentine: I. In: Proceedings of the 12th national conference on clays and clay minerals, Atlanta, Georgia, September 30–October 2, 1963. Atlanta, Georgia; 1964. p. 35–47, 49–54.
[57] Gualtieri AF, Giacobbe C, Viti C. The dehydroxylation of serpentine group minerals. Am Miner 2012;97:666–80.
[58] MacKenzie KJD, Meinhold RH. Thermal reactions of chrysotile revisited: a 29Si and 25 Mg MAS NMR study. Am Miner 1994;79:43–50.
[59] Martin CJ. The thermal decomposition of chrysotile. Miner Mag 1977;41:453–9.
[60] MacKenzie KJD, Meinhold RH. 25Mg nuclear magnetic resonance spectroscopy of minerals and related inorganics: a survey study. Am Miner 1994;79:250–60.
[61] Chizmeshya AVG, McKelvy MJ, Wolf GH, Carpenter RW, Gormley DA, Diefenbacher JR, et al. Enhancing the atomic-level understanding of CO_2 mineral sequestration mechanisms via advanced computational modeling: final report. Tempe, Arizona: Center for Solid State Science, Arizona State University; 2006.
[62] Balucan RD, Kennedy EM, Mackie JF, Dlugogorski BZ. Optimization of antigorite heat pre-treatment via kinetic modeling of the dehydroxylation reaction for CO_2 mineralization. Greenh Gas Sci Technol 2011;1:294–304.
[63] McKelvy MJ, Chizmeshya AVG, Diefenbacher J, Bearat H, Wolf G. Exploration of the role of heat activation in enhancing serpentine carbon sequestration reactions. Environ Sci Technol 2004;38:6897–903.
[64] McKelvy MJ, Sharma R, Chizmeshya AVG, Carpenter RW, Streib K. Magnesium hydroxide dehydroxylation: in-situ nanoscale observations of lamellar nucleation and growth. Chem Mater 2001;13:921–6.
[65] MacKenzie KJD, McGavin DG. Thermal and Mossbauer studies of iron-containing hydrous silicates. Part 8 Chrysotile. Thermochim Acta 1994;244: 205–21.
[66] Coats CJA. Serpentine minerals from Manitoba. Can Miner 1968;9:322–47.
[67] Perez-Rodriguez JL, Franco F, Ramirez-Valle V, Perez-Maqueda LA. Modification of the thermal dehydroxylation of antigorite by ultrasound treatment. J Therm Anal Calorim 2005;82:769–74.
[68] Chizmeshya AVG, McKelvy MJ, Adams JB. Atomic-level modeling of CO_2 disposal as carbonate mineral: a synergetic approach to optimizing reaction process design. Tempe, AZ: Arizona State University; 2001.
[69] Chizmeshya AVG, McKelvy MJ, Sharma R, Carpenter RW, Bearat H. Density functional theory study of the decomposition of $Mg(OH)_2$: a lamellar dehydroxylation model. Mater Chem Phys 2002;77:416–25.
[70] Llana-Funez S, Brodie KH, Rutter EH, Arkwright JC. Experimental dehydration kinetics of serpentine using pore volumetry. J Metamorph Geol 2007;25: 423–38.
[71] Alizadehhesari K, Golding SD, Bhatia SK. Kinetics of the dehydroxylation of serpentine. Energy Fuels 2012;26:783–90.
[72] Vyazovkin S, Dollimore D. Linear and non-linear procedures in isoconversional computations of the activation energy of non-isothermal reactions in solids. J Chem Inf Comput Sci 1996;36:42–5.
[73] Vyazovkin S, Wight C. Model-free and model-fitting approaches to kinetic analysis of isothermal and nonisothermal data. Thermochem Acta 1999;340–341:53–68.
[74] Vyazovkin S, Clawson J, Wight C. Thermal dissociation kinetics of solid and liquid ammonium nitrate. Chem Mater 2001;13:960–6.
[75] Butt DP, Lackner KS, Wendt CH, Conzone SD, Kung H, Lu Y, et al. Kinetics of thermal dehydroxylation and carbonation of magnesium hydroxide. J Am Ceram Soc 1996;79:1892–8.
[76] Brown ME. Introduction to thermal analysis: techniques and applications. 2nd ed.. New York, USA: Kluwer Academic Publishers; 2001.
[77] Drief A, Nieto F. The effect of dry grinding on antigorite from Mulhacen, Spain. Clay Clay Miner 1999;47(4):417–24.
[78] Franco F, Perez-Maqueda L, Ramirez-Valle V, Perez-Rodriguez J. Spectroscopic study of the dehydroxylation process of sonicated antigorite. Eur J Miner 2006;18:257–64.
[79] Govier D, Arnold M. Quantitative differential thermal analysis of antigorite and lizardite serpentine: internal report. Albany Research Center Analytical Laboratory; 2004.
[80] O'Connor WK, Dahlin DC, Rush GE, Gerdemann SJ, Penner LR. Energy and economic considerations for ex-situ aqueous mineral carbonation, DOE/ARC-2004-028. Albany, Oregon: U.S. Department of Energy, Albany Research Center; 2004.
[81] Fedoročková A, Hreus M, Raschman P, Sučik G. Dissolution of magnesium from calcined serpentinite in hydrochloric acid. Miner Eng 2012;1:1–4.
[82] Ghoorah M, Dlugogorski BZ, Oskierski H, Kennedy EM. Weak acid-induced dissolution of thermally conditioned serpentinites for carbon dioxide mineralisation. Miner Eng, in review.
[83] Fouda MFR, Amin RE, Abd-Elzaher MM. Extraction of magnesia from Egyptian serpentine ore via reaction with different acids: I: reaction with sulfuric acid. Bull Chem Soc Jpn 1996;69:1907–12.
[84] O'Connor WK, Dahlin DC, Nilsen RP, Rush GE, Walters RP, Turner PC. Carbon dioxide sequestration by direct mineral carbonation: results from recent studies and current status. In: 1st Annual DOE carbon sequestration conference, DOE/ARC-2001-029. Washington, D.C.: National Energy Technology Laboratory, United States Department of Energy; May 14–17, 2001.
[85] Maroto-Valer MM, Fauth DJ, Kuchta ME, Zhang Y, Andresen JM. Activation of magnesium rich minerals as carbonation feedstock materials for CO_2 sequestration. Fuel Process Technol 2005;86:1627–45.
[86] O'Connor WK, Dahlin DC, Nilsen RP, Gerdemann SJ, Nilsen RP. Aqueous mineral carbonation: mineral availability, pretreatment, reaction parametrics, and process studies, DOE/ARC-TR-04-002. Albany, Oregon: Albany Research Center; 2005.
[87] Li W, Li W, Li B, Bai Z. Electrolysis and heat pretreatment methods to promote CO2 sequestration by mineral carbonation. Chem Eng Res Des 2009;87:210–5.
[88] Penner L, O'Connor WK, Dahlin DC, Gerdemann S, Rush GE. Mineral carbonation: energy cost of pre-treatment options and insights gained from flow loop reaction studies. In: 3rd annual conference on carbon capture & sequestration, DOE/ARC-2004-042. Alexandria, VA, May 3–6, 2004. Alexandria, VA; 2004.
[89] Podschus E, Bayerwick L, Joseph W. Treatment of silicates. United States Patent Office. Patent No.3,021,195; 1962.
[90] Brent G. Integrated chemical process. Patent WO/2008/0631305 A1; 2008.
[91] Geerlings JJC, Wesker E. Process for sequestration of carbon dioxide by mineral carbonation. United States Patent. Patent No. US7,722,850 B2; 2010.
[92] Boerrigter, H. Process for preparing an activated mineral. United States Patent. Patent No. US2010/0282079 A1; 2010.
[93] Chizmeshya AVG, Brent GF. High-temperature treatment of hydrous minerals. Patent WO 2011/035047 A2; 2011.